Poriferal Vision: Classifying Benthic Sponge Spicules to Assess Historical Impacts of Marine Climate Change

Saketh Saxena[1], Philip Heller[1](✉), Amanda S. Kahn[2], and Ivano Aiello[2]

[1] San Jose State University, San Jose, CA 95192, USA
philip.heller@sjsu.edu
[2] Moss Landing Marine Laboratories, Moss Landing, CA 95039, USA

Abstract. Sponges and corals are ecologically important members of the marine community. Climate change, while harmful to corals, has historically been favorable to sponges. Sponge population dynamics are studied by analyzing core samples of marine sediment. To date this analysis has been performed by microscopic visual inspection of core cross sections to distinguish spicules (the rigid silica components of sponge skeletons) from the residue of other silica-using organisms. Since this analysis is both slow and error prone, complete analysis of multiple cross sections is impossible.

FlowCam® technology can produce tens of thousands of microphotographs of individual core sample particles in a few minutes. Individual photos must then be classified *in silico*. We have developed a Deep Learning classifier, called Poriferal Vision, that distinguishes sponge spicules from non-spicule particles. Small training sets were enhanced using image augmentation to achieve accuracy of at least 95%. A Support Vector Machine trained on the same data achieved accuracy of at most 86%. Our results demonstrate the efficacy of Deep Learning for analyzing core samples, and show that our classifier will be an effective tool for large-scale analysis.

Keywords: Deep Learning · Sponges · Porifera · Climate

1 Introduction

Sponges (Phylum Porifera) are prolific reef builders [1] and benthic grazers [2, 3]. Many sponges (Phylum Porifera, especially Classes Demospongiae and Hexactinellida) form spicules – the rigid components of their skeletons – composed of silica. Since silica can resist breakdown for millions of years, spicules are part of the geological record, providing insight into the presence and ecological significance of sponges under a variety of climatic conditions. Sponge populations have increased significantly during planetary warm periods, including the Upper Carboniferous period (300 mya) [4], some stages of the Paleozoic (540–250 mya) and Mesozoic (250–65 mya) eras [5], the Triassic/Jurassic transition (200 mya) [6], and the Pliocene warm period (3 mya) [7].

D. Helic et al. (Eds.): ISMIS 2020, LNAI 12117, pp. 205–213, 2020.
https://doi.org/10.1007/978-3-030-59491-6_19

Shallow water reefs are hotspots of marine biodiversity, fringing 1/6 of the world's coastlines [8] and supporting hundreds of thousands of species [9]. Reefs are predominantly coral rather than sponge; the hard carbonate exoskeletons of dead coral polyps accrete to form non-living support structures for living reef components. However, coral reefs are particularly vulnerable to current climate change conditions. Rising temperatures cause bleaching by forcing expulsion of heat-intolerant symbionts [10, 11]. Ocean acidification, driven by increased CO2 in the atmosphere, slows production of calcium carbonate and accelerates removal of calcium carbonate by dissolution and bioerosion [12–14] in shallow and deep waters; moreover there is mounting evidence that increasing acidity disrupts the life cycle of corals at multiple stages [15]. Goreau et al. have estimated that climate change had destroyed or degraded 25% of all reefs by the year 2000 [16]. The loss of coral reefs can be expected to continue through the century, since atmospheric CO2 levels are expected to rise to 750 ppm by 2100 [17].

The ongoing degradation of coral reefs, together with the historical success of sponges during warm periods, suggest that sponges may be due for a resurgence in ecological importance, and may replace corals as major reef builders [18]. The ecological and economic importance of reefs motivate research into the mechanics of the historical success of sponges during past warm periods. Although glass sponges do not build significant shallow water reefs, they are similar to reef-building corals in that they form the foundation for unique communities [19], provide three-dimensional habitat [20], are a nursery habitat for many species [21], and enhance local biodiversity [19, 22]. Their historical response to climate change can therefore elucidate present-day coral and sponge population dynamics. Much information can be gained by counting and classifying spicules from smear slides of spicule-bearing core samples (Fig. 1).

Unfortunately, while particle size distribution can be computed mechanically, identification of particles is labor intensive. Core sections must be inspected microscopically, and spicules must be distinguished from the organic and inorganic constituents of the cores, plus refractory detritus of other silica-using organisms such as diatoms and radiolarians (Phylum Retaria). Comprehensive analysis of large numbers of sections is not practical. FlowCam® technology (Fluid Imaging Technologies, Inc.) offers a partial solution to this problem of scale. In a FlowCam device, particles in suspension pass one by one in front of a camera; this approach can generate tens of thousands of photographs from a sample in a matter of minutes. To our knowledge this technology has not yet been systematically applied to core samples, although recent success with cyanobacterial blooms [23] suggests that the approach is promising. However, a FlowCam approach to large-scale spicule analysis requires software classification of large numbers of individual photographs. To facilitate development of a classifier, Fluid Imaging Technologies generously performed a small-scale run on a core sample from the Bering Sea from the Pliocene warm period. 110 photographs of sponge spicules and 113 photographs of non-spicule particles (diatoms and radiolarians) were generated (Fig. 1).

Our experience with computer vision technology suggested that an accurate photograph classifier could be achieved using Artificial Neural Networks (ANNs), which have been shown to be effective in handling large scale image classification problems and are the de-facto standard in image recognition problems [24, 25]. In particular we hypothesized that a deep convolutional neural network (ConvNet) [26] could achieve

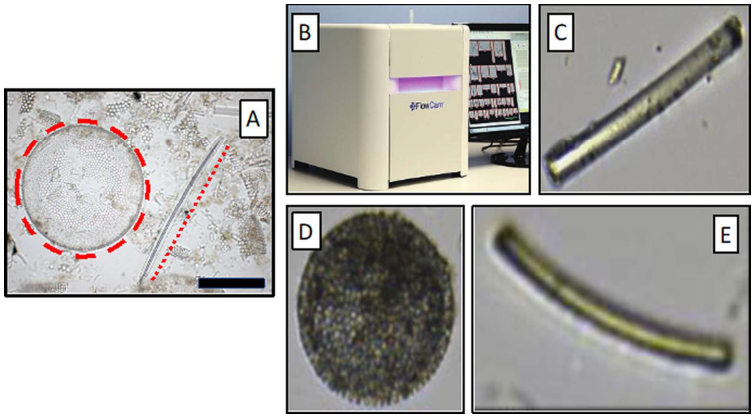

Fig. 1. (A) Smear slide microphotograph showing a diatom (in red dashed circle) and a glass sponge spicule (along dashed red line). (B) FlowCam series 8000 flow imaging microscope. Reprinted with permission from Fluid Imaging Technologies, Inc. (C) Glass sponge spicule. (D) Diatom. (E) Radiolarian. The similarity between (C) and (E) necessitates a sophisticated software classifier. (Color figure online)

acceptable accuracy despite the obvious similarity between glass sponge spicules and radiolarians. However, ConvNets require extensive positive training data, and the available training data consisted of just 110 positive examples and 113 negative examples from the few FlowCam images provided by Fluid Imaging Technologies. Fortunately, training data can be enhanced *in silico*, and we further hypothesized that ConvNet accuracy could benefit from data augmentation [27] via image manipulation of the original photographs. We have trained a deep ConvNet, called "Poriferal Vision", that achieves 95% accuracy with available data. A Support Vector Machine (SVM) classifier [28, 29] was trained using the same data to provide a basis for comparison; the Poriferal Vision model consistently achieved higher accuracy.

2 Methods

To enable rapid *in silico* identification of FlowCam images from marine core samples, a deep convolutional neural network (ConvNet) called "Poriferal Vision" was trained on data from the Bering Sea. Data augmentation was applied to training instances. 20% of the augmented data was withheld from training and used for testing. Withheld data was tested on the Poriferal Vision ConvNet and, for comparison, on a Support Vector Machine.

2.1 Data Collection

Sediments from a section of a Bering Sea core sample (Fig. 3) were provided by the Aiello research group at Moss Landing Marine Laboratories. The Integrated Ocean Drilling Program Expedition 323 to the Bering Sea (IODP Exp 323) discovered that, in the central part of this marginal sea at Bowers Ridge (Site U1340, ~600 m; water depth 1295 m; Fig. 3), sponge spicules comprise a very important component of hemipelagic sedimentation, together with diatom frustules and ice-rafted debris (Fig. 2) [7, 30].

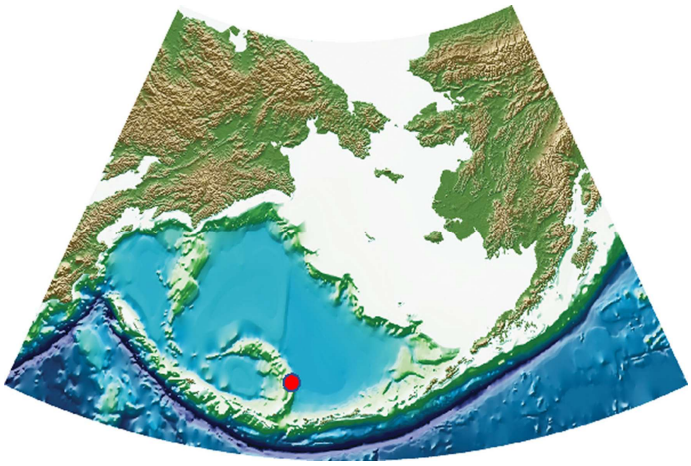

Fig. 2. Bering Sea and adjacent landmasses. The red dot marks sampling site U1340. (Color figure online)

To create positive training and testing sets, 110 sponge spicule photographs were manually selected. Negative example photographs of 80 diatoms and 33 radiolarians were collected. All photographs were randomly split into training and testing sets. To compensate for the small number of training examples, the positive and negative training sets were enhanced by transforming images using the OpenCV software package [31]. Individual images were read into OpenCV in grayscale. In order to preserve the structure of the single objects in the photos and to get more realistic transformations, the polygonal chain approximation method [32] was used to trace highly accurate contours around each object. A rectangular bounding box was drawn around the contours, isolating the object and preserving its local background context. The bounding box was flipped horizontally, vertically, and horizontally + vertically to generate 3 new images from each original. All images were rotated in increments of 15°. Lastly, in order to reduce the probability of misidentification of poorly centered images, 6 perspective transformations were applied to each original image by translating the object by a small distance. To ensure that perspective transformation did not create any blank images, a blurring Gaussian filter [33] was applied to the transformed images; any image with a majority of black pixels or a majority of white pixels was removed from the data set. All image backgrounds were cleaned by removing noise and deleting line artifacts of rotation. Images were saved in .jpg format and, as a quality control check, visually inspected. Accepted images were resized to 138 × 78 pixels (the mean resolution among accepted images).

2.2 ConvNet and Support Vector Machine Design and Training

The Poriferal Vision ConvNet was implemented in TensorFlow [34]; The architecture of the model was conservatively inspired by AlexNet [26], which seems suitable as a pioneering large scale image classification architecture for our specific problem. The motivation behind designing a lean ConvNet was to accommodate for the limited size of the dataset despite data augmentation and learn a generalizable distribution of features from it. It consists of two 2D convolutional layers with a filter size of 64 and kernel size of (3, 3) to convolve over. Considering the relatively small dimension of the transformed images a smaller kernel size would allow learning localized features and differentiate

between spicules and radiolarians, due to the high degree of similarity between them. Both layers use relu [35] activation function and max pooling to down sample the input representation.

These are followed by a flatten and dense layer with relu activation to reduce the spatial dimension of the input, finally followed by an output layer with sigmoid activation [36] (Fig. 3). Training proceeded for 14 epochs.

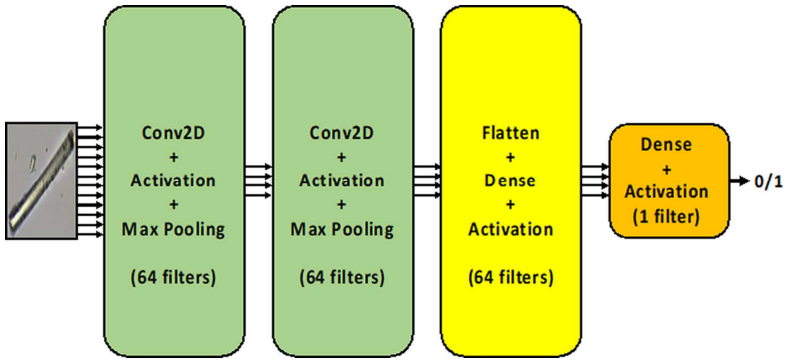

Fig. 3. Poriferal Vision Convolutional Neural Network (CNN) design

To provide a basis for assessing the Poriferal Vision model, a Support Vector Machine classifier was created using the Support Vector Classifier module of SciKit-Learn [37], with a linear kernel. Following the method of R. Sahak et al. [38], training time was reduced by using Principal Component Analysis (PCA) to limit feature dimensionality. The kernel's c and gamma parameters were optimized using SciKit-Learn's GridSearchCV module.

2.3 Evaluation

The Poriferal Vision ConvNet was trained first with the original training data and then with the enhanced data. In each category (sponge spicules, diatoms, and radiolarians), 20% of data was withheld from training and later used for testing (Table 1). All training and experiments performed on Poriferal Vision were also performed on the Support Vector Machine. For all 4 experiments (Poriferal Vision and SVM, original and enhanced data), the classifiers were evaluated by computing test accuracy, f-score, precision, and recall.

Table 1. Training and testing sets.

Data Set	Organism	Original photos	Original testing photos	Original training photos	Flipped images	Rotated images	Perspective transformations	Total selected training images
Positive	Sponges	110	30	80	240	5120	376	5816
Negative	Diatoms	90	22	68	204	4352	408	5032
	Radiolarians	33	8	25	75	1600	150	1850

3 Results

Test accuracy, f-score, precision, and recall for the 4 experiments are given in Table 2. Accuracy and loss over 14 training epochs, for both the original and enhanced data sets, are shown in Fig. 4.

Table 2. Results for SVM and Poriferal Vision, for original and enhanced (i.e. original and transformed) images.

Model	Images	Test accuracy	F-score	Precision	Recall
SVM	Original	0.83	0.83	0.83	0.83
	Enhanced	0.80	0.79	0.86	0.80
Poriferal Vision	Original	0.92	0.92	0.93	0.92
	Enhanced	0.95	0.95	0.95	0.95

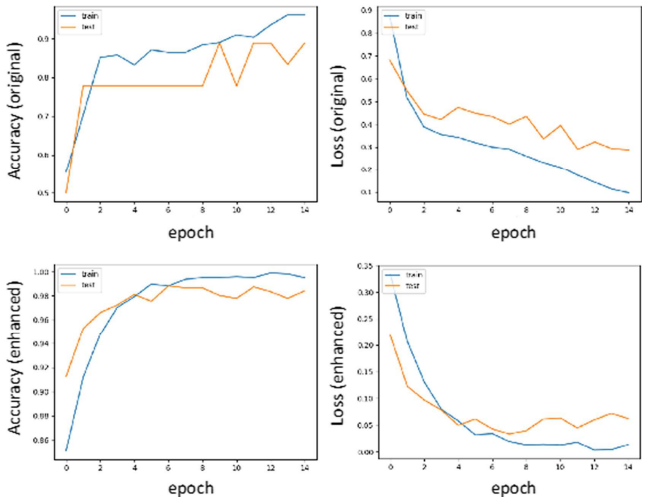

Fig. 4. Poriferal Vision CNN training regimes, showing accuracy (left) and loss (right) with the original (top) and enhanced (bottom) data sets over 14 training epochs. The test set (brown lines) was composed of 20% of each photograph set (spicules, diatoms, radiolarians), selected randomly and withheld from model training. (Color figure online)

4 Discussion

The Poriferal Vision ConvNet, trained with the enhanced data set, achieved 95% accuracy according to all 4 computed statistics (test accuracy, f-score, precision, and recall). Enhancing the positive and negative training data added 2–3% to the statistics. Our hypotheses are therefore confirmed: a ConvNet has been shown to achieve reasonable accuracy, and image enhancement improves accuracy. Significantly, the enhanced-data version of Poriferal Vision is accurate enough to be applied to large-scale sets of FlowCam images when those become available.

The Support Vector Machine classifiers, trained on the same data as the Poriferal Vision models, was less accurate than Poriferal Vision by 5 to 11% points. This may be due to the PCA-based dimension reduction which was applied in order to make model computation time tractable. The time complexity of a linear kernel SVM is O(n), where n is the number of dimensions. Since SVMs are not practical without dimension reduction, they are not appropriate for the kind of classification undertaken here.

The next stage of Poriferal Vision's development will involve taxonomic classification of spicules (and perhaps diatoms and radiolarians). We hope and expect that the insights gained from consequent analysis of the historical record will help the scientific and ocean policy communities to understand the future role of sponges in marine environments.

5 Conclusions

The Poriferal Vision ConvNet, trained with the enhanced data set, achieved at least 95% accuracy according to all 4 computed statistics (test accuracy, f-score, precision, and recall). This result justifies future efforts to expand the training set.

A larger training set, with spicules identified by species or by higher taxonomic level, will enable a more sophisticated classifier that can identify samples by species or by higher taxonomic level. Such a classifier, if deployed on shipboard and receiving FlowCam images in real time, would enable real-time analysis of the local marine environment, thus greatly enhancing the efficiency of sponge analysis at a moment in human history when such analysis is urgent.

References

1. Conway, K.W., Barrie, J.V., Krautter, M.: Geomorphology of unique reefs on the western Canadian shelf: sponge reefs mapped by multibeam bathymetry. Geo-Mar. Lett. **25**(4), 205–213 (2005)
2. Yahel, G., Whitney, F., Reiswig, H.M., Eerkes-Medrano, D.I., Leys, S.P.: In situ feeding and metabolism of glass sponges (Hexactinellida, Porifera) studied in a deep temperate fjord with a remotely operated submersible. Limnol. Oceanogr. **52**(1), 428–440 (2007)
3. Kahn, A.S., Yahel, G., Chu, J.W.F., Tunnicliffe, V., Leys, S.P.: Benthic grazing and carbon sequestration by deep-water glass sponge reefs. Limnol. Oceanogr. **60**(1), 78–88 (2015)
4. West, R.R.: Temporal changes in Carboniferous reef mound communities. PALAIOS **3**(2), 152 (1988)
5. Brunton, F.R., Dixon, O.A.: Siliceous sponge-microbe biotic associations and their recurrence through the phanerozoic as reef mound constructors. PALAIOS **9**(4), 370 (1994)
6. Kiessling, W., Simpson, C.: On the potential for ocean acidification to be a general cause of ancient reef crises: ancient reef crises. Glob. Change Biol. **17**(1), 56–67 (2011)
7. Aiello, I.W., Ravelo, A.C.: Evolution of marine sedimentation in the Bering Sea since the Pliocene. Geosphere **8**(6), 1231–1253 (2012)
8. Birkeland, C. (ed.): Life and Death of Coral Reefs. Chapman and Hall, New York (1997)
9. Reaka-Kudla, M.L., Wilson, D.E., Wilson, E.O.: Biodiversity II. Joseph Henry Press, Washington, D.C. (1997)
10. Glynn, P.W.: Coral reef bleaching: ecological perspectives. Coral Reefs **12**(1), 1–17 (1993). https://doi.org/10.1007/BF00303779

11. Hughes, T.P.: Climate change, human impacts, and the resilience of coral reefs. Science **301**(5635), 929–933 (2003)
12. De'ath, G., Fabricius, K.E., Sweatman, H., Puotinen, M.: The 27-year decline of coral cover on the Great Barrier Reef and its causes. Proc. Natl. Acad. Sci. **109**(44), 17995–17999 (2012)
13. Hoegh-Guldberg, O., et al.: Coral reefs under rapid climate change and ocean acidification. Science **318**(5857), 1737–1742 (2007)
14. Wisshak, M., Schönberg, C.H.L., Form, A., Freiwald, A.: Ocean acidification accelerates reef bioerosion. PLoS ONE **7**(9), e45124 (2012)
15. Albright, R.: Reviewing the effects of ocean acidification on sexual reproduction and early life history stages of reef-building corals. J. Mar. Biol. **2011**, 1–14 (2011)
16. Goreau, T., McClanahan, T., Hayes, R., Strong, A.: Conservation of coral reefs after the 1998 global bleaching event. Conserv. Biol. **14**(1), 5–15 (2000)
17. Nakićenović, N., Intergovernmental Panel on Climate Change (eds.): Special Report on Emissions Scenarios: A Special Report of Working Group III of the Intergovernmental Panel on Climate Change. Cambridge University Press, Cambridge, New York (2000)
18. Bell, J.J., Davy, S.K., Jones, T., Taylor, M.W., Webster, N.S.: Could some coral reefs become sponge reefs as our climate changes? Glob. Change Biol. **19**(9), 2613–2624 (2013)
19. Chu, J., Leys, S.: High resolution mapping of community structure in three glass sponge reefs (Porifera, Hexactinellida). Mar. Ecol. Prog. Ser. **417**, 97–113 (2010)
20. Beaulieu, S.E.: Life on glass houses: sponge stalk communities in the deep sea. Mar. Biol. **138**(4), 803–817 (2001)
21. Marliave, J.B., Conway, K.W., Gibbs, D.M., Lamb, A., Gibbs, C.: Biodiversity and rockfish recruitment in sponge gardens and bioherms of southern British Columbia, Canada. Mar. Biol. **156**(11), 2247–2254 (2009)
22. Guillas, K.C., Kahn, A.S., Grant, N., Archer, S.K., Dunham, A., Leys, S.P.: Settlement of juvenile glass sponges and other invertebrate cryptofauna on the Hecate Strait glass sponge reefs. Invertebr. Biol. **138**(4), e12266 (2019)
23. Graham, M.D., et al.: High-resolution imaging particle analysis of freshwater cyanobacterial blooms: FlowCam analysis of cyanobacteria. Limnol. Oceanogr. Methods **16**(10), 669–679 (2018)
24. Widrow, B., Rumelhart, D.E., Lehr, M.A.: Neural networks: applications in industry, business and science. Commun. ACM **37**, 93–106 (1994)
25. Rawat, W., Wang, Z.: Deep convolutional neural networks for image classification: a comprehensive review. Neural Comput. **29**(9), 2352–2449 (2017)
26. Krizhevsky, A., Sutskever, I., Hinton, G.E.: ImageNet classification with deep convolutional neural networks. Commun. ACM **60**(6), 84–90 (2017)
27. Shorten, C., Khoshgoftaar, T.M.: A survey on image data augmentation for deep learning. J. Big Data **6**(1), 1–48 (2019). https://doi.org/10.1186/s40537-019-0197-0
28. Cortes, C., Vapnik, V.: Support-vector networks. Mach. Learn. **20**(3), 273–297 (1995)
29. Chapelle, O., Haffner, P., Vapnik, V.N.: Support vector machines for histogram-based image classification. IEEE Trans. Neural Netw. **10**(5), 1055–1064 (1999)
30. Schlung, S.A., et al.: Millennial-scale climate change and intermediate water circulation in the Bering Sea from 90 ka: a high-resolution record from IODP Site U1340: Bering Sea climate change since 90 KA. Paleoceanography **28**(1), 54–67 (2013)
31. Bradski, G.R., Kaehler, A.: Learning OpenCV: Computer Vision with the OpenCV Library, 1st edn. O'Reilly, Beijing (2011)
32. Ramer, U.: An iterative procedure for the polygonal approximation of plane curves. Comput. Graph. Image Process. **1**(3), 244–256 (1972)
33. Deng, G., Cahill, L.W.: An adaptive Gaussian filter for noise reduction and edge detection. In: 1993 IEEE Conference Record Nuclear Science Symposium and Medical Imaging Conference (1993)

34. Abadi, M., et al.: TensorFlow: a system for large-scale machine learning, p. 21 (2016)
35. Hahnloser, R.H.R., Sarpeshkar, R., Mahowald, M.A., Douglas, R.J., Seung, H.S.: Digital selection and analogue amplification coexist in a cortex-inspired silicon circuit. Nature **405**, 947–951 (2000)
36. Kilian, J., Siegelmann, H.T.: The dynamic universality of sigmoidal neural networks. Inf. Comput. **128**(1), 48–56 (1996)
37. Pedregosa, F., et al.: Scikit-learn: machine learning in Python. J. Mach. Learn. Res. **12**, 2825–2830 (2011)
38. Sahak, R., Mansor, W., Lee, Y.K., Yassin, A.I.M., Zabidi, A.: Performance of combined support vector machine and principal component analysis in recognizing infant cry with asphyxia. In: 2010 Annual International Conference of the IEEE Engineering in Medicine and Biology (2010)